Improving the efficiency of photodetector structures based on Ge/Si quantum dots by photonic crystal modes in the mid-infrared range

© A.A. Bloshkin[1,2], A.I. Yakimov[1]

[1] Rzhanov Institute of Semiconductor Physics, Siberian Branch, Russian Academy of Sciences,
630090 Novosibirsk, Russia
[2] Novosibirsk State University,
630090 Novosibirsk, Russia

E-mail: bloshkin@isp.nsc.ru

Received April 10, 2025
Revised June 18, 2025
Accepted July 29, 2025

The spatial distribution of the electromagnetic field of a light wave in Ge/Si heterostructures with Ge quantum dots on a silicon-on-insulator substrate coupled to a photonic crystal has been studied using mathematical modeling methods. The array of air holes served to convert the radiation incident along the normal to the surface into planar waveguide modes. The period of the photonic crystal ranged from 1.3 to 1.8 microns, the hole depth ranged from 100 to 1100 nm, and the hole diameter was 2/3 of the period of the structure. A series of optical resonances with multiple (up to 300 times) amplification of the intensity of the light wave field in the quantum dot layers in the wavelength range of 2–6 microns compared with the structure without holes has been detected. The optimal parameters of the structure (the period of the photonic crystal and the depth of the holes) have been determined, ensuring maximum amplification of the photo response.

Keywords: Ge/Si quantum dots, photonic crystal, waveguide modes, electric field enhancement.

DOI: 10.61011/SC.2025.04.61723.7801

1. Introduction

Detection of middle infrared band (IRB) electromagnetic radiation is one of the priority tasks of the physics of semiconductors and semiconductor devices. Wavelength range of light, $3-5\,\mu$m, is of interest for gas and aerosol detection in atmosphere [2], various medical applications [2] and detection of objects being of interest for the military. Medium IRB photodetectors (PD) were implemented on the basis of various materials and structures such as indium antimonide [3–6], $Ga_xAl_{1-x}As$-quantum wells [6], Ge/Si quantum dots (QD) [7–9], heterojunctions in nitrides of group III elements [10]. Ge/Si heterostructures with Ge QD are of particular interest among all components for detecting medium IRB radiation owing to their compatibility with extensively developed silicon technology. When creating matrix PD on such structures, it is possible to use monolithic integration of a signal multiplexing circuit and active radiation detection region on a single substrate, offering a considerable reduction of a finished product cost. Another important factor of monolithic integration of PD on silicon substrate is the formation of an ultrahigh-resolution PD due to currently existing commercially available Si substrates with a diameter > 300 mm, while substrates with a diameter ≤ 100 mm are available for other materials.

Low quantum efficiency of light absorption in quantum dots due to a low density of quantum dots is the main disadvantage of Ge/Si QD PD. Typical ampere-watt sensitivity of a QD photodetector is $0.2-0.8$ mA/W at $3-5\,\mu$m [8,9]. At the same time, structures based on interband transitions in indium antimonide demonstrate a sensitivity of 0.6 to 0.8 A/W in the same wavelength range [11]. If the efficiency of conversion of medium IRB electromagnetic radiation into electric current in Ge/Si QD PD could be increased considerably, then this would allow commercial implementation of matrix detector on the basis of such structures. Some success in this area was achieved when using a plasmon wave near field occurring at the interface between the semiconductor matrix and metallic film [12,13]. At the same time to increase the near infrared efficiency of Ge/Si QD, an approach was developed where silicon-on-insulator (SOI) substrates were used for structure formation. When using such substrates, the photodetector's active region was formed in a Si layer localized between the buried SiO_2 layer and air above the structure surface. This layer consists of a planar waveguide where various light modes may propagate along the waveguide surface. To convert the incident light incoming normally to the structure surface into the light propagating parallel to the surface in the waveguide layer, periodic diffraction structures are used that have been recently called photonic crystals (PC) [14–16]. When QDs are placed in the waveguide layer region, the efficiency of interaction between the quantum dots and electromagnetic wave field increases due to an increase in the electric field intensity and in the optical path of light passing through the active medium. In visible and near IRB, periodic arrays of holes are extensively used as photonic crystals for increasing light efficiency of quantum dots [17–22]. Meanwhile, there is virtually no literature concerning the use of PC to increase the medium IRB light efficiency or absorption.

The aim of this work was to use mathematical simulation for identifying potential applicability of photonic crystal

structures for localization and amplification of medium IRB electromagnetic radiation in waveguide layers with Ge/Si quantum dots formed on the SOI substrates.

2. Model

Three-dimensional electromagnetic field was calculated using the finite element method in the frequency region. This method was implemented in Comsol Multiphysics software package using the „Wave Optics“ module [23]. Simulation region consisted of a parallelepiped whose width and depth were defined by the photonic crystal period, and the parallelepiped height was defined by the total thickness of layers involved in the calculation. There was a SOI substrate with a SiO_2 $2\,\mu$m buried layer and 110 nm surface Si layer in the parallelepiped base. SiO_2 and surface Si layer thicknesses were chosen on the basis of commercially available substrates for structure growth [24]. The main mechanism of medium IR photocurrent generation in Ge/Si QD is associated with hole transitions from localized states in QD to the Si valence band and further hole drift to contact regions. Therefore the active region of a standard structure optimized for radiation detection consists of a pair of p^+ type contacts placed above and below the QD layers [8,25,26]. The p^+-Si bottom layer thickness was set to 200 nm because of the process constraints in manufacturing of real structures, the top layer thickness was 100 nm. A region occupied by quantum dots consisted of a stack of 15 QD layers separated by 40 nm Si interlayers. Total thickness of the QD-occupied region was 600 nm. This region was separated from the contact layers by two undoped Si layers: 200 nm layer at the bottom and 120 nm layer at the top. The total Si layer thickness above the buried SiO_2 was 1330 nm. A simple evaluation of the maximum wavelength of radiation that may propagate in such waveguide gives $\sim 8\,\mu$m [27], which is higher than the upper boundary of the atmospheric transparency window of $3-5\,\mu$m. To convert radiation normally incoming to the structure surface into the radiation propagating in the waveguide region, a diffraction structure consisting of a periodic array of air holes is used. The array period w varied within $1.3-1.8\,\mu$m, the hole diameter d was 1.5 times smaller than the period. The hole depth h varied from 100 to 1100 nm in 100 nm intervals. The structure is shown schematically in Figure 1.

The model used linear electromagnetic radiation polarization with the electric field vector **E** directed along the x axis. The incident electromagnetic wave propagated normally to the structure surface (along the z axis). Simulation was performed in the wavelength range of $\lambda = 2-6\,\mu$m. In this range, the photoconductivity of Ge/Si heterostructures with Ge quantum dots is induced by optical transitions from the levels in quantum dots to the valence band states [28]. Since quantum dots occupy a small fraction of the structure volume ($< 1\,\%$), and the optical constants of Si and Ge in this spectral range are close to each other [29], then particular properties of quantum dots such as size or density were not considered in the simulation. Light absorption efficiency in semiconductor heterostructures with QDs is proportional to the squared electric field intensity in the region occupied by quantum dots [15]. To determine the influence of the photonic crystal on the light absorption efficiency, a dimensionless electric field intensity amplification factor β was used:

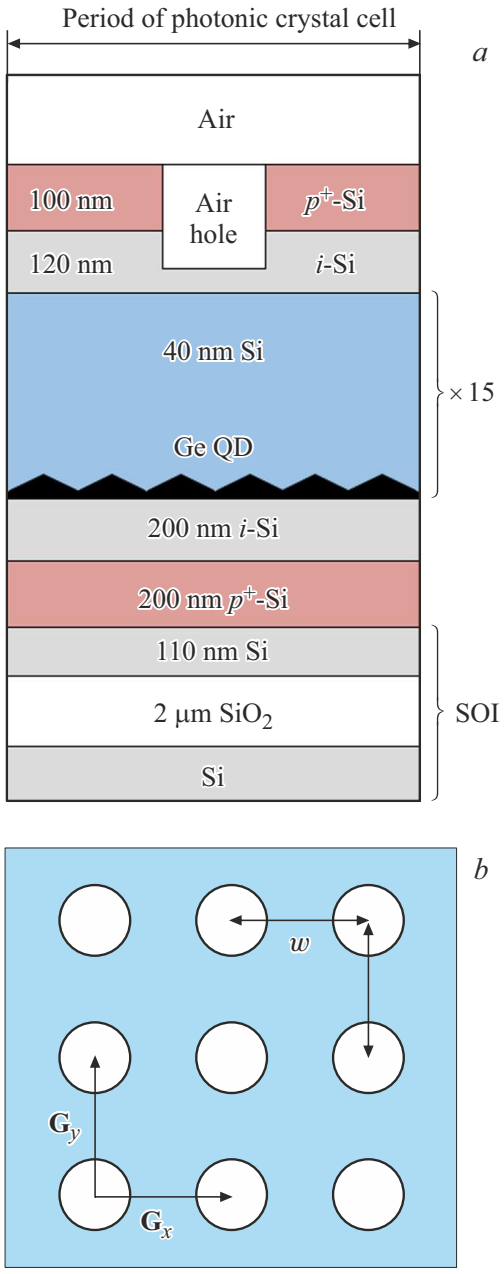

Figure 1. *a* — schematic diagram of the simulated structure. *b* — plan view of the simulated array of holes that served as a photonic crystal. Single vectors of the reciprocal photonic crystal lattice $\mathbf{G}_x$, $\mathbf{G}_y$ are shown schematically. The photonic crystal period w varied from 1.3 to 1.8 μm, the hole diameter was 2/3 of the period, the depth varied from 100 to 1100 nm.

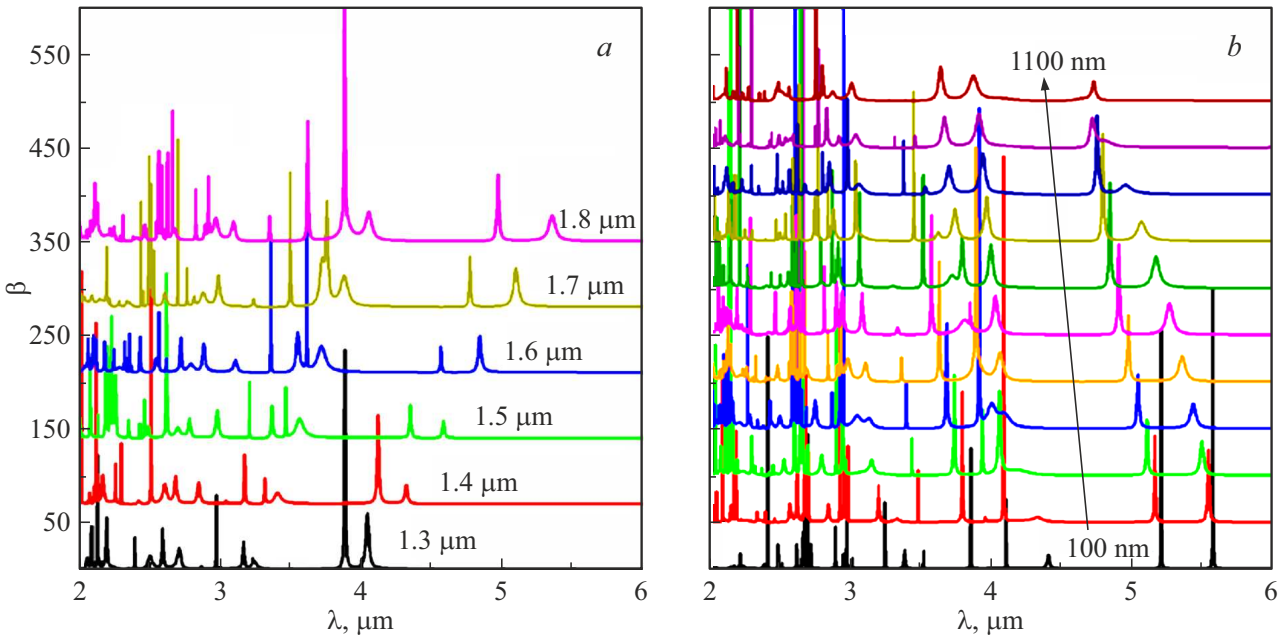

Figure 2. β for the hole depth of 500 nm and different structure periods (a), and for a fixed period of 1.8 μm and hole depths of 100, 200, 300, 400, 500, 600, 700, 800, 900, 1000 and 110 nm (b).

$$\beta = \frac{\int_{V_{QD}} |E_{PC}|^2 \, dV}{\int_{V_{QD}} |E_{\text{ref}}|^2 \, dV}. \quad (1)$$

Here, E_{PC} and E_{ref} are electric fields in the structure with the photonic crystal and in the structure without air holes, integration is performed in the region V_{QD} containing Ge quantum dots.

3. Results

Figure 2 shows the simulation of the electric field intensity amplification factor for the hole depth $h = 500$ nm and different photonic crystal periods (Figure 2, a) and for $w = 1.8\,\mu$m with different hole depths (Figure 2, b). It is shown that the amplification factor has a clearly pronounced resonance structure where the base peak positions vary when the parameters of the surface array of holes are varied. As the photonic crystal period increases with a permanent hole depth, the peak positions shift to the long-wavelength spectrum region. As the hole depth increases, the peak positions shift backwards. When the hole depth is 100 nm, the amplification factor curve has a form of a set of narrow resonance peaks whose amplitude reaches 300. As the hole depth increases, a decrease in the amplification factor and line width growth are observed. These effects may be explained by classical diffraction theory. Let's consider an electromagnetic wave incoming from air with the refractive index n_{Air} onto the interface with Si whose refractive index is $n_{\text{Si}} > n_{\text{Air}}$. Suppose there is a periodic array of holes having a square lattice symmetry with the square side w. Then for light that can propagate on Si, the following conditions shall be satisfied:

$$\mathbf{k}_{\text{Si}} = \mathbf{k} \pm \mathbf{G}, \quad (2)$$

$$\mathbf{G} = \frac{2\pi m_x}{w}\,\mathbf{e}_x + \frac{2\pi m_y}{w}\,\mathbf{e}_y. \quad (3)$$

Here, $\mathbf{k}$ is the incident wave vector, $\mathbf{k}_{\text{Si}}$ is the wave vector of the wave propagation via the waveguide, $\mathbf{G}$ is the arbitrary vector of the reciprocal lattice of the surface structure, m_x, m_y are integers denoting the mode number, $\mathbf{e}_x$, $\mathbf{e}_y$ are the unit coordinate vectors. Taking into account that $|k_{\text{Si}}| = 2\pi n_{\text{Si}}/\lambda$ and $|k| = 2\pi/\lambda$, the following results are obtained: as w grows, the reciprocal lattice vector decreases in modulus with fixed m_x and m_y, therefore, to satisfy condition (2), $\mathbf{k}$ and $\mathbf{k}_{\text{Si}}$ shall decrease in modulus. Specifically, the radiation wavelength at which the waveguide modes are excited shall grow.

Note that a part of the volume is occupied by air with other refractive index. The Bruggeman model is one of the main effective refractive index calculation models for two media occupying comparable volume fractions f_1 and f_2 such that $f_1 + f_2 = 1$ [30]. Within the effective medium model, as the air fraction increases, the effective permittivity together with the effective refractive index decrease. Therefore, with a fixed reciprocal lattice vector, k_{Si}, at which resonance is observed, grows. While the wavelength decreases, accordingly.

To determine the optimum structure parameters it was decided to use the integral amplification parameter that is

calculated as follows

$$\gamma(h, w) = \int_{\lambda_1}^{\lambda_2} \beta(h, w, \lambda) d\lambda. \quad (4)$$

Here, $\lambda_1 = 2$, $\lambda_2 = 6\,\mu$m are the boundaries of the wavelength range, in which the electric field amplification is considered. This parameter characterizes full sensitivity of the photodetector structure. Optical response from Ge quantum dots is observed in this wavelength range in real structures [28]. Figure 3 shows the dependence of the integral amplification parameter on the hole depth with different photonic crystal periods. The figure shows that the maximum integral amplification parameter occurs at periods $> 1.6\,\mu$m and in the hole depth range from 0.2 to $0.4\,\mu$m. Moreover, the curves show that, as the structure period increases, the integral amplification parameter increases with a fixed hole depth.

The reason for such behavior of the amplification factor may be understood from the following considerations. 1) As the structure period increases, the growing number of modes of the photonic crystal fall within this frequency band. Further increase in the period will not give such effect any longer because the most long-wavelength mode will start going out of the chosen wavelength range and getting into the Ge QD dead zone. 2) As the hole depth increases, the efficiency of conversion of the incident electromagnetic wave energy into diffraction modes increases compared with the fundamental mode passing into the substrate. However, if the hole depth > 300 nm, then the hole starts entering the active region of the structure occupied by quantum dots and, thus, reduces the region volume, in which β is

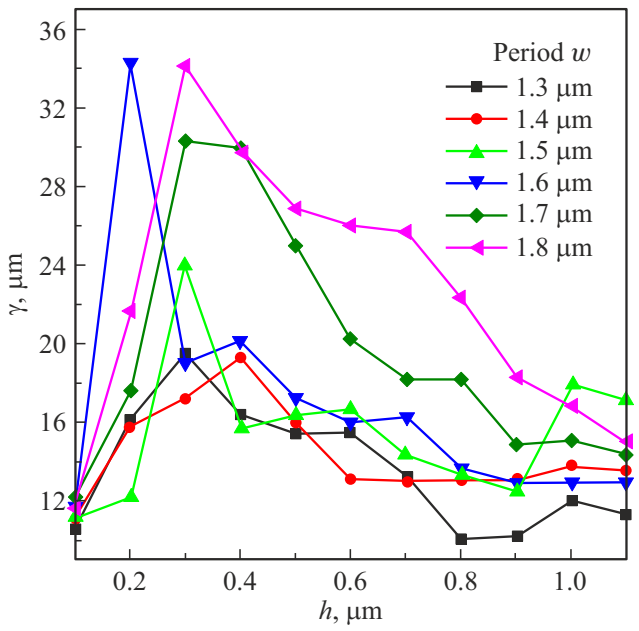

Figure 3. Integral parameter of electric field intensity amplification in the active region of the photodetector structure vs. the hole depth.

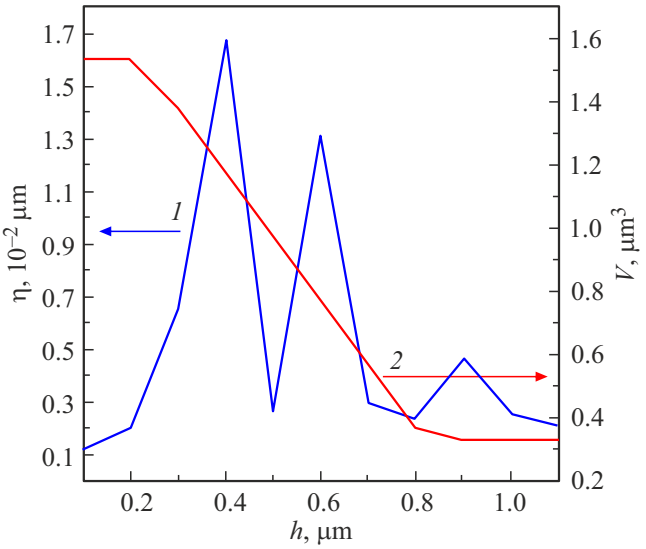

Figure 4. Integral efficiency of conversion of the incident radiation energy into the planar waveguide modes (curve *1*) for the structure with the photonic crystal period equal to $1.6\,\mu$m and the active region volume (curve *2*) vs. the hole depth.

calculated. Thus, competition of two processes starts at depths > 300 nm: on the one hand, an increase in the hole depth increases the efficiency of conversion of the incident radiation into photonic crystal modes, and, on the other hand, it reduces the volume of region, from which an effective signal may be acquired. With the hole depth $> 0.9\,\mu$m, the active region volume stops decreasing, the region has been passed completely and behavior of γ with the increase in the period is already defined by other factors. This work didn't address these factors because the efficiency of these hole depths is in any case much lower than that of the depth of $0.2-0.4\,\mu$m.

Efficiency of conversion of the incident radiation energy into the lateral waveguide modes may be described using the relation of the energy flux through the side surface of the waveguide to the power W of the light wave incoming onto the structure. Energy flux Φ through the side surface S_{side} was calculated as

$$\Phi = \int_{S_{\text{side}}} \mathbf{P}\, d\mathbf{S}. \quad (5)$$

Here, $\mathbf{P}$ is the Poynting vector, $d\mathbf{S}$ is the external normal to the side surface of the waveguide lattice cell. Integral efficiency of conversion of the incident radiation into the waveguide modes was calculated in the entire waveguide range as follows

$$\eta(h, w) = \int_{\lambda_1}^{\lambda_2} \frac{\Phi(h, w, \lambda)}{W} d\lambda. \quad (6)$$

Figure 4 shows the dependence of $\eta(h)$ for the structure period of $1.6\,\mu$m (black curve, left y axis) and the active

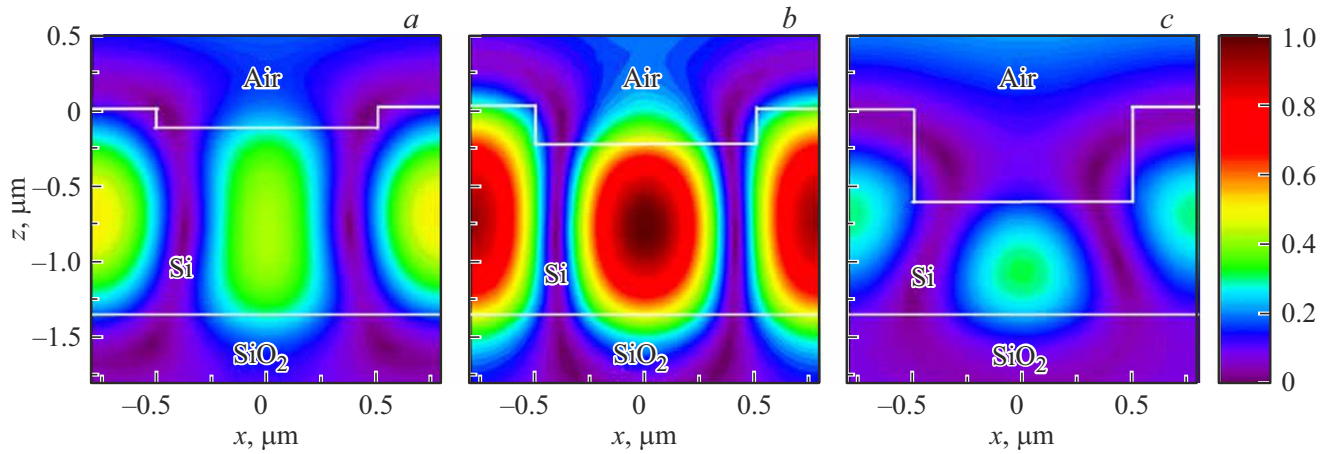

Figure 5. Spatial distribution of the electric field in the fundamental waveguide mode for the photonic crystal with a period of 1.6 μm and hole depth of 100 (*a*), 200 (*b*), 600 (*c*) nm. A wavelength, for which the distributions were plotted, was 5.018 μm, 4.997 μm and 4.989 μm, respectively.

region volume V (red curve, right y axis) on the hole depth. The curve shows that, with hole depths $< 0.4\,\mu$m, efficiency of conversion increases monotonously as the hole depth increases. With further growth of the hole depth, oscillating behavior of $\eta(h)$ is observed, but the maximum efficiency decreases in this case. Meanwhile, the active region volume decreases monotonously as the hole depth increases. Thus, the maximum of the integral field amplification parameter $\gamma(h)$ shall be within the depth range from 0.2 to 0.4 μm. For the period of 1.6 μm, the maximum is observed for $h = 0.2\,\mu$m.

For better illustration of our hypothesis concerning the variation of the efficiency of the incident radiation energy into the photonic crystal modes as the hole depth varies, a spatial distribution of the electric field in the observed fundamental mode of the photonic crystal was plotted. Figure 5 shows the distribution of component E_y for the photonic crystal with a period of 1.6 μm and three different hole depths: 100 nm, 200 nm and 600 nm. A wavelength, for which the distributions were plotted, was 5.018 μm, 4.997 μm and 4.989 μm, respectively. It can be seen from the electromagnetic field distribution that the electric field amplitude first grows as the hole depth increases from 100 nm to 200 nm, and then the amplitude of E_y decreases gradually.

4. Conclusion

Mathematical modelling methods were used to show that the medium IRB electromagnetic wave intensity in Ge/Si quantum dot layers may be increased considerably by the modes of a photonic crystal formed on the heterostructure surface. The photonic crystal consists of a periodic array of subwavelength air holes. It was found that the growth of intensity of some photonic crystal modes might increase by 300 times on a quantum dot. A characterization method was proposed for the integral efficiency of photodetector structures in the chosen wavelength range. It is shown that, for all photonic crystal periods, the dependence of the integral amplification parameter on the hole depth has its maximum at 0.2−0.4 μm. It was found that structures with the photonic crystal period of 1.6−1.8 μm and hole depths of 0.2−0.4 μm should be used for the maximum light amplification efficiency in the wavelength range of 2−6 μm.

Funding

The study was carried out under the state assignment of the Ministry of Science and Higher Education of the Russian Federation (topic No. FWGW-2025-0023, Control of functional properties of nanophtonic and nanoelectronic components based on semiconductor nanostructures).

Conflict of interest

The authors declare that they have no conflict of interest.

References

[1] C. Clerbaux, A. Boynard, L. Clarisse, M. George, J. Hadji-Lazaro, H. Herbin, D. Hurtmans, M. Pommier, A. Razavi, S. Turquety, C. Wespes, P.-F. Atmos. Chem. Phys., **9**, 6041 (2009).
[2] E.F.J. Ring, K. Ammer. Physiol. Meas., **33**, R33 (2012).
[3] H. Menon, H. Jeddi, N.P. Morgan, A. Fontcuberta i Morral, H. Pettersson, M. Borg. Nanoscale Adv., **5**, 1152 (2023).
[4] I. Kimukin, N. Biyikli, T. Kartaloğlu, O. Aytür, E. Ozbay. IEEE J. Select. Top. Quant. Electron., **10**, 766 (2004).
[5] B.W. Jia, K.H. Tan, W.K. Loke, S. Wicaksono, K.H. Lee, S.F. Yoon. ACS Photonics, **5**, 1512 (2018).
[6] F.D.P. Alves, J. Amorim, M. Byloos, H.C. Liu, A. Bezinger, M. Buchanan, N. Hanson, G. Karunasiri. J. Appl. Phys., **103**, 114515 (2008).

[7] N. Rappaport E. Finkman, T. Brunhes, P. Boucaud, S. Sauvage, N. Yam, V. Le Thanh, D. Bouchier. Appl. Phys. Lett., **77**, 3224 (2000).
[8] A.I. Yakimov, V.A. Timofeev, A.A. Bloshkin, A.I. Nikiforov, A.V. Dvurechenskii. Nanoscale Res. Lett., **7**, 494 (2012).
[9] A.I. Yakimov, A.A. Bloshkin, V.A. Timofeev, A.I. Nikiforov, A.V. Dvurechenskii. Appl. Phys. Lett., **100**, 10 (2012).
[10] L.K. Wu, H.L. Hao, W.Z. Shen. J. Appl. Phys., **103**, 044507 (2008).
[11] A. Dehzangi, D. Wu, R. McClintock, J. Li, M. Razeghi. Appl. Phys. Lett., **116**, 221103 (2020).
[12] A.I. Yakimov, V.V Kirienko, A.A. Bloshkin, V.A. Armbrister, A.V. Dvurechenskii. J. Appl. Phys., **122**, 133101 (2017).
[13] A.I. Yakimov, V.V. Kirienko, A.A. Bloshkin, V.A. Armbrister, A.V. Dvurechenskii, J.-M. Hartmann. Opt. Express, **25**, 25602 (2017).
[14] A.I. Yakimov, V.V. Kirienko, A.A. Bloshkin, D.E. Utkin, A.V. Dvurechenskii. Photonics, **10**, 764 (2023).
[15] A.I. Yakimov, A.A. Bloshkin, V.V. Kirienko, A.V. Dvurechensky, D.E. Utkin. Pisma ZhETF **113**, 501 (2021). (in Russian).
[16] A.I. Yakimov, V.V. Kirienko, A.V. Dvurechensky, D.E. Utkin. Pisma ZhETF **240**, 2023 (2017). (in Russian).
[17] M. Calic, C. Jarlov, P. Gallo, B. Dwir, A. Rudra, E. Kapon. Sci. Rep., **7**, 1 (2017).
[18] I. Söllner, S. Mahmoodian, S.L. Hansen, L. Midolo, A. Javadi, G. Kiršanskė, T. Pregnolato, H. El-Ella, E. H. Lee, J. D. Song, S. Stobbe, P. Lodahl. Nature Nanotechnol., **10**, 775 (2015).
[19] M. Schatzl, F. Hackl, M. Glaser, P. Rauter, M. Brehm, L. Spindlberger, A. Simbula, M. Galli, T. Fromherz, F. Schäffler. ACS Photonics, **4**, 665 (2017).
[20] X. Xu, N. Usami, T. Maruizumi, Y. Shiraki. J. Cryst. Growth, **378**, 636 (2013).
[21] Z.V. Smagina, V.A. Zinoviev, A.F. Zinovieva, M.V. Stepikhova, A.V. Peretokin, E.E. Rodyakina, S.A. Dyakov, A.V. Novikov, A.V. Dvurechenskii. J. Luminesc., **249**, 119033 (2022).
[22] R. Shankar, R. Leijssen, I. Bulu, M. Lončar. Opt. Express, **19**, 5579 (2011).
[23] Comsol Multiphysics software. http://comsol.com
[24] V.A. Zinovyev, M.V. Stepikhova, Zh.V. Smagina, A.A. Bloshkin, E.E. Rodyakina, M.S. Mikhailovskii, A.V. Novikov. J. Appl. Phys., **136**, 153103 (2024).
[25] A.I. Yakimov, V.A. Timofeev, A.A. Bloshkin, V.V. Kirienko, A.I. Nikiforov, A.V. Dvurechenskii. J. Appl. Phys., **112**, 034511 (2012).
[26] A.I. Yakimov, A.A. Bloshkin, V.A. Timofeev, A.I. Nikiforov, A.V. Dvurechenskii. Appl. Phys. Lett., **100**, 053507 (2012).
[27] N.V. Nikonorov, S.M. Shandarov *Volnovodnaya fotonika* (SPb., SPbGU ITMO 2008). (in Russian).
[28] A.I. Yakimov, V.A. Timofeev, A.A. Bloshkin, V.V. Kirienko, A.I. Nikiforov, A.V. Dvurechenskii. J. Appl. Phys., **112**, 034511 (2012).
[29] H.H. Li. J. Phys. Chem. Ref. Data, **9 (3)**, 561 (1980). DOI: 10.1063/1.555624
[30] D.A.G. Bruggeman. Ann. Phys., **421**, 160 (1937).

Translated by E.Ilinskaya